Polarization-Based Angle Sensitive Pixels for Light Field Image Sensors With High Spatio-Angular Resolution

Vigil Varghese and Shoushun Chen, *Senior Member, IEEE*

***Abstract*— This paper presents a new angle sensitive pixel design for use in light field image sensors. This new pixel, referred to as the macro-pixel, is comprised of seven sub-pixels, and can determine the light angles in the range from $-45°$ to $+45°$. The range of detectable angles is only limited by the presence of routing metals in the vicinity of the pixels. Each macro-pixel captures incident light angle through the aid of sub-wavelength metallic structures at its focal plane. Unlike previous designs that needed a large number of sub-pixels to determine a limited range of the incident angles, the presented design requires only half as many sub-pixels while offering a comparatively large angle detection range.**

***Index Terms*— Polarization pixels, angle detection, quadrature pixel cluster, light field image sensor, linear angle sensitive pixels, Talbot pixels.**

I. Introduction

LIGHT field image sensors are back in prominence because of the commercial demands for 3D imaging and post capture image refocus. Commercial light field cameras are inspired by the principles of integral photography laid out by Lippmann [1] and Ives [2].

Integral photography, also known as multi-aperture imaging [3], [4] or plenoptic imaging uses two sets of lenses to recreate the visual information available in the imaged scene. The first lens, commonly referred to as the objective or main lens helps in focusing the light on to the focal plane of a set of micro-lenses. Each micro-lens captures a small collection of light rays from a particular part of the main lens and re-sorts them into bins by means of a number of sub-pixels underneath each micro-lens. By performing displacement analysis of all the sub-images from the sub-pixels we can reconstruct a rich image which contains more information about the imaged scene as compared with a traditional camera.

The additional information contained in the captured image enables applications such as post capture image refocus [5], synthetic aperture photography [6], multi-viewpoint visualization [7], 3D imaging [7], [8], among others. The angular resolution of multi-aperture camera is limited by the number of sub-pixels underneath each micro-lens and the spatial resolution is limited by the number of micro-lenses in the imager array [6]. The inherent trade-off in multi-aperture cameras is intertwined between that of spatial resolution and angular resolution. We cannot increase one without decreasing the other for any practical size image sensor array.

Increasing the number of micro-lenses increases the spatial resolution of the captured image, but for a reasonable amount of sub-pixels, would require a large imager array, which is technologically challenging. On the other hand, a large angular resolution would require a large number of sub-pixels below each micro-lens, which reduces the spatial resolution. Hence, we are in search of a technique which provides appreciable spatial resolution without sacrificing much of the angular resolution. That is, a technique that does not have an inherent trade-off like the multi-aperture camera.

Albert Wang, et al., in their seminal work on diffraction based Talbot effect [9], [10] demonstrated a technique for capturing the incident light angle using a group of angle sensitive pixels known as Talbot pixels. This technique was based on using the CMOS metal layer stack as on-chip diffraction grating which facilitates encoding the incident angle of light as intensity variations in the pixel. A number of applications were demonstrated [11]–[14] to illustrate the usefulness of the technique and were in tune with what we expect from the additional light field information.

While the technique was successful in eliminating the inherent trade-off present in the multi-aperture imaging technique, use of diffraction gratings introduced additional complications. Firstly, the response - a result of the Talbot effect [15], is periodic in nature. Decoding a single angle from such a periodic sequence requires a number of similar periodic sequences, each shifted by an appropriate offset. Secondly, the Talbot pixels are direction sensitive, i.e., a horizontal Talbot pixel can only detect angle variations along the vertical direction and vice versa. Thirdly, there exits a trade-off between angle sensitivity and detectable angle range. The parameters of the Talbot gratings can be adjusted to increase one or the other. A consequence of all these limitations is that we end up using a large number of pixels to decode angle variations (32 to be precise, for horizontal and vertical angle variations) and it involves non-trivial post-processing.

Earlier attempts to overcome this limitation focused on combining different pixel types to achieve a higher spatial resolution, while maintaining an appreciable angular resolution.

One such technique [16] - the track and tune image sensor, was based on using the metal shading based [17], [18] quadrature pixel cluster [19] in order to achieve a high spatial resolution (13 pixels for bi-directional angle detection) while enabling a wide angular resolution ($\pm 35°$). The essence of the track-and-tune technique was to use a group of pixels with low sensitivity, but high linearity (quadrature pixel cluster) along with another group of pixels with high sensitivity, but low linearity (Talbot pixels) to determine the local incidence angle.

Keeping in line with this trend of using disparate pixel types as a group to determine local incidence angle we propose using polarization pixels instead of Talbot pixels [20] for achieving a better spatio-angular resolution. In this new technique we use a group of polarization pixels with different directional polarization gratings for determining local incidence angle with high sensitivity. Although the polarization pixels are highly sensitive to variations in local incidence angles, the response is symmetrical around 0°. That is, it is not possible to identify whether the angle is either positive or negative. In order to break the symmetry we use another set of pixels, the quadrature pixel cluster, to obtain a low sensitive, linear response. This linear response helps us to differentiate between the positive and negative angles of the polarization pixels and in conjunction with it helps to obtain a sensor with high spatio-angular resolution.

The main contribution of this paper is the introduction of a new technique based on polarization to determine the local incidence angle at each macro-pixel. This technique facilitates a higher spatial resolution of the light field sensor by employing only a small number of pixels (7 in total, compared to the 32 required for Talbot only solution [9]) for bi-directional angle detection. Moreover, the range of angles that can be uniquely detected is also higher (greater than 70°, compared to 20° from the Talbot sensor), which could be useful in lens-less imaging applications.

Section II sheds light on the polarization property of light and the techniques to detect the same. Section III examines the angle sensitive nature of polarization pixels and presents a technique to determine local incidence angle. Section IV goes through the design of the prototype sensor and touches upon the various design parameters. Section V illustrates the test setup and briefs about the testing methodology. Section VI introduces experimental results and section VII provides a discussion of the non-idealities. We conclude by justifying the need for this new technique and contrasting it with the earlier ones in section VIII.

II. Polarization and Its Detection

Polarization is a property of Electro-Magnetic (EM) waves (which includes visible light) in which the electric field (or magnetic field) has preference for vibration along a particular orientation.

EM waves are said to be unpolarized or randomly polarized (Fig. 1a) if the electric field does not have any preference for vibration along a particular orientation. On the other hand, if the electric field is confined to vibrate along a particular orientation, the light is said to be linearly polarized. EM waves are said to be partially polarized (Fig. 1b) if they have a

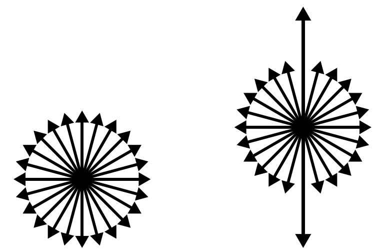

(a) (b)

Fig. 1. Figure showing electric-field vector orientation of randomly polarized light (a) and partially polarized light (b) with its major component oriented along the 90° axis.

predominant electric field component with a well defined vibration axis, along with other minor components along random orientations. Majority of man-made light sources are partially polarized [21]. Sun light gets partially polarized due to scattering on passing through earth's atmosphere. Light can also become polarized as a result of reflection from dielectric surfaces and refraction on passing through certain birefringent materials such as calcite.

Many animals have the ability to detect the polarization state of light in their natural habitats. Some arthropods like cray-fish [22], [23], spider [24], desert ant [25], desert locust [26] and certain vertebrates like lizards [27] and salmon [28] are known to make use of polarization information in their surroundings for either egocentric navigation [29] or secondary vision that assists in polarization contrast imaging. Although humans have a well developed vision that detects variations in color and brightness over several orders of magnitude, they are incapable of detecting the polarization information.

Literature abounds with the many applications that are enabled by the capture of polarization information. Material classification [30], [31], navigation [32], polarization contrast imaging of biological tissues [33], non-contact latent fingerprint imaging [34], enhancing vision under hazy conditions [35], 3D object recognition [36] and many others. All these applications are enabled by the ability to detect the polarization information through CCD or CMOS cameras [37]. In order to make an ordinary imager detect polarization information, we need to augment them with special optics, known as polarizers.

Polarization state of the light can be detected by using an image sensor with pixels capable of producing response proportional to the polarization state. Division-of-time, division-of-focal-plane [38] and division-of-amplitude [39] are the prominent techniques for polarization detection using a CMOS/CCD image sensor. Division-of-time polarization imaging is realized by using a rotating polarizer in front of the imager and capturing the image for each orientation of the polarizer in a time multiplexed manner. Multiple images must be captured and processed to determine the polarization state of the incident light. The main drawback of this technique is time aliasing for scenes with object motion or brightness variations.

Division-of-amplitude polarization imaging uses beam splitters and retarders along with two or more image sensors to capture the polarization information. Requirement of additional optical components and precise alignment of the optical setup is a serious limitation with this technique.

Division-of-focal-plane polarization imaging is realized by having polarization sensitive gratings on top of the pixel in the focal plane of the sensor. Neighboring pixels have gratings with different orientations and adjacent pixels work as a group to determine the local polarization information. The drawback here is a reduction in spatial resolution that is dependent on the number of grating orientations that are being realized in the pixel array.

Division-of-focal-plane polarization imaging is almost always preferred because of the above mentioned issues related to division-of-time and division-of-amplitude polarization imaging; even at the cost of reduced spatial resolution. This shift is also rendered possible by the miniaturization of pixel geometry as a result of technology scaling and the subsequent improvements in optical lithography enabling fabrication of polarizers with sufficiently small dimensions.

Traditionally, division-of-focal-plane polarizers consisted of polarization gratings made of poly vinyl alcohol (PVA) polymers, birefringent crystals or Aluminum nano-wires which were deposited on top of pixels from commercial CCD or CMOS image sensors through post-CMOS fabrication process. Usually multiple sheets of polarizer films had to be placed to achieve multiple polarizer orientations [37]. This reduced the light transmission onto the photodiode, making signal detection challenging. These multiple sheets placed at a considerable height above the photodiode surface also increased pixel crosstalk leading to a reduction in the polarization extinction ratio (PER - is a measure of the quality of the polarizer) of the polarizer. PER is also sensitive to the alignment between the pixel and the polarizer sheets and care must be taken to avoid any misalignment. The cost for such a polarization imager increases as a result of all the post processing operations.

With the rapid scaling of CMOS technology over the past decade, implementing polarizer gratings monolithically on top of the pixel has become an option. These gratings are implemented in the metal layers of the CMOS process stack. This requires no additional post processing steps and careful design can reduce pixel crosstalk. However, unlike other techniques mentioned above, the on-chip polarizers generally tend to have a low extinction ratio. As the technology continues to scale and the minimum required metal width decreases, the extinction ratio will become large enough to be useful for a wide variety of polarization applications.

Figure 2 shows randomly polarized light being horizontally polarized as a result of it passing through a vertical wire-grid polarizer. When a randomly polarized light is incident on a wire-grid polarizer, all the components of the electric field along the orientation of the polarizer will be blocked by it while the components orthogonal to the polarizer orientation will be allowed to pass through.

A polarizer grating can be characterized by its width 'W' and pitch 'd'. From theory [40] we know that a wire grid grating such as the one shown in figure 2 is capable of exhibiting polarization properties if $\lambda > 2d$, where λ is the wavelength of the incident light. In the 65 nm CMOS process, the minimum width of the metal 1 (M1) layer is 90 nm, which gives a minimum pitch of 180 nm. From the above equation we could infer that such a polarizer grating would exhibit strong polarization response for wavelengths above 360 nm. Since the visible range is roughly from 300 nm to 700 nm, we can use this polarizer in the visible range for detecting the polarization state of the incoming light.

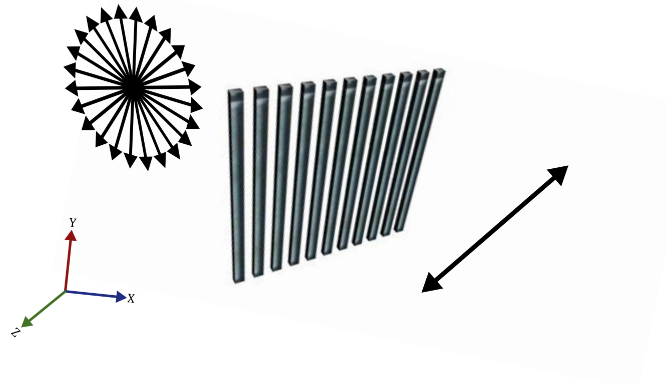

Fig. 2. Figure showing unpolarized light being horizontally polarized by a vertical polarization grating.

Earlier works [41], [42] have shown the effect of varying the polarizer parameters and its impact on the polarization extinction ratio. For our design we have chosen to implement the polarizer grating using the metal 1 layer with a pitch of 200 nm and 50% duty cycle.

III. Incident Light Angle Detection

Being able to detect the direction of the incoming light ray allows one to capture more complete information about the imaged scene [9] as opposed to the conventional cameras that capture only brightness (intensity) and color (wavelength). This complete description of light, known as the light field [43], describes light at a point in space as a function of position and direction. In regions free of occluders, the light field can be described by a 4 dimensional function, known as the plenoptic function [44], [45], [46]. The four parameters of the function x, y, V_x and V_y represent the x, y coordinate direction in the object plane and the V_x, V_y viewing direction in the image plane. By capturing the light ray direction we essentially capture the V_x and V_y parameters, with the x and y coordinates of the pixel array giving the other two parameters.

Capturing the light field information allows an image sensor to have additional capabilities such as post capture refocus [47], [48], depth map computation [46], vision through occluders [48], [49], among others. The price that has to be paid for these additional capabilities is a reduction in sensor resolution as additional pixels are required for decoding the angle information.

As mentioned in the introduction, one of the first techniques that enabled light angle detection at the pixel level was the Talbot pixel. The following subsection gives a brief overview of the angle sensitive Talbot pixels. For a more complete description the reader is encouraged to refer [9], [16] or [50].

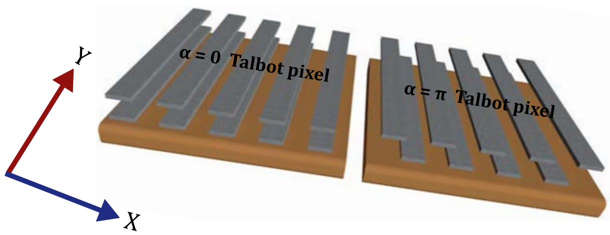

Fig. 3. Physical structure of vertical Talbot pixels.

A. Angle Sensitive Talbot Pixels

Talbot pixels use diffraction based Talbot effect [15] to detect the incoming light ray direction. It uses two pairs of diffraction gratings made of metal layers from the CMOS process stack on top of the photodiode. The first layer, called the primary, produces self-images of the gratings at multiples of depth $z_t/2$, where $z_t=2d^2/\lambda$, with 'd' being the grating pitch and 'λ' being the wavelength of light. The second layer, called the secondary, is placed at a depth of $z_t/2$ or its multiples and acts as a mask either blocking or passing light through it onto the photodiode. The self images projected from the primary onto the secondary shifts linearly with the changes in the incident light angle. This effect, called the off-axis Talbot effect [51], is the guiding principle leading to the angle sensitive nature of the Talbot pixels.

Figure 3 shows the physical structure of two Talbot pixels. The secondary grating in the left pixel is placed directly below the primary grating, i.e., there is no offset (denoted by α) between the primary and the secondary gratings. On the other hand, the secondary grating in the right pixel is placed in the gaps left by the primary gratings at a depth $z_t/2$ and here the offset between the primary and the secondary grating is d/2 or $\alpha = \pi$. At a minimum, two different pixels with two grating offsets of $\alpha = 0$ and π are required to make sure that light of higher intensity at an angle blocked by the secondary and light of lower intensity at an angle passed by the secondary do not produce ambiguous response. The difference response of these two pixels are used for angle detection.

The response produced by a Talbot pixel can be described by [9, Equation 1]. I_0 is the intensity of the incident light onto the primary grating, 'm' is the strength of the response, β_T is angle sensitivity, θ is the incident angle and α is the grating offset.

$$I = I_0(1+m\cos(\beta_T\theta+\alpha)) \tag{1}$$

Figure 4 shows the finite difference time domain (FDTD) simulation of the difference response produced by a pair of Talbot pixels subjected to plane wave illumination at a wavelength of 600 nm, sampled at 5° increments from −45° to +45°. Gratings with a pitch of 0.76 um and a duty cycle of 50% were used for the simulation. As one would expect based on equation 1, the response is cosine in nature with 'm' and 'β_T' determined by grating parameters of pitch, 'd', and vertical grating separation, $z_t/2$.

The difference Talbot response is periodic, with the range of uniquely detectable angles around 10°. In order to determine a larger range of angles we need to have additional Talbot

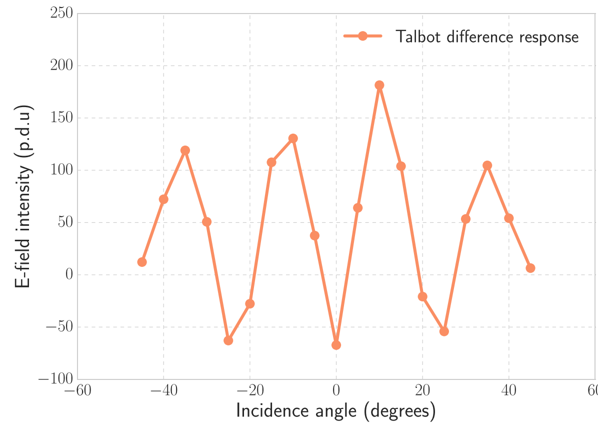

Fig. 4. Difference Talbot response produced by Talbot pixels with grating offsets of $\alpha = 0$ and π.

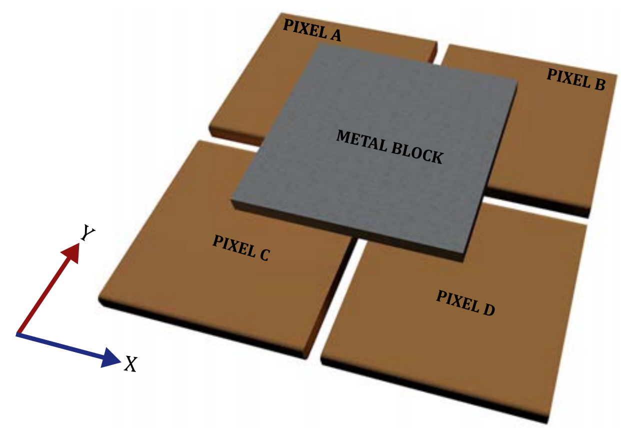

Fig. 5. Physical structure of quadrature pixel cluster (QPC) pixels.

pixels with different grating parameters that produce response with different angular sensitivities (β_T). Also, as mentioned earlier, the Talbot pixels are direction sensitive, and hence can only detect angle variations that are orthogonal to the grating orientation. Overall, using only Talbot pixels to determine the incident light angle requires a total of 32 pixels [9] for horizontal and vertical angle variations.

B. Quadrature Pixel Cluster

In [16] and [19] we proposed an alternative approach to the Talbot-only technique of angle detection. We proposed to combine the response from the Talbot pixels with the response from a quadrature pixel cluster (QPC). A quadrature pixel cluster is a set of four pixels with a metal block on top that symmetrically covers a part of each pixel as shown in figure 5.

When the incident light is normal to the pixel plane all the pixels receive the same amount of light and hence the difference response between pixels is zero. When the light is incident at an angle to the normal, say from left to right along the X-axis, pixels A and C receive more light than pixels B and D. On the other hand, when the light direction is from right to left, pixels B and D receive more light than

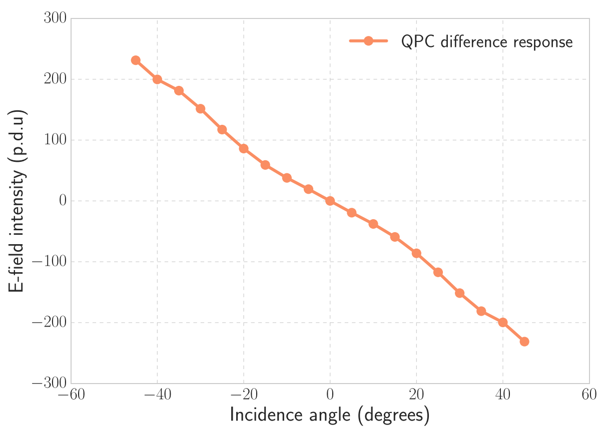

Fig. 6. Difference response produced by QPC pixels (A, B or C, D) when incident light angle is varied along the X axis.

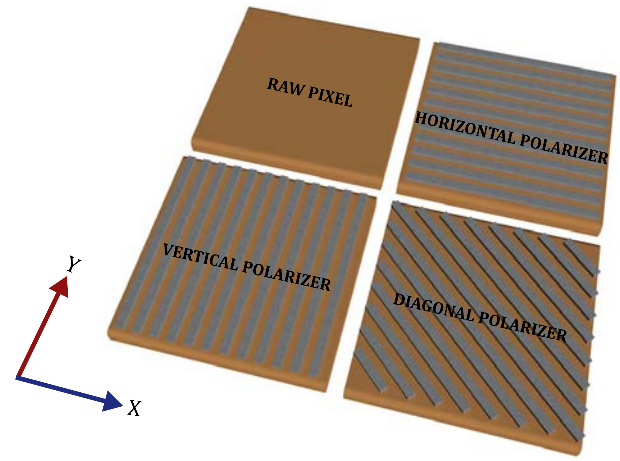

Fig. 7. Physical structure of single-layer polarization pixels.

pixels A and C. By taking the difference response between pixels A or C and pixels B or D we can determine the incident light angle. This difference response is shown in the plot (Fig. 6), which is from a FDTD simulation.

Although the difference response is linear in nature the angle sensitivity of the response is low and coupled with sensor noise would render detecting only big changes in angles feasible. This is why we combined the linear response from QPC pixels with the non-linear, highly sensitive response from Talbot pixels to detect the incident light angles at a higher spatial resolution and with a lower post processing complexity.

C. Angle Sensitive Polarization Pixels

We make use of the angle sensitive nature of the polarizers to design a polarization pixel cluster (Fig. 7) with three different grating orientations for detecting incident light angles. The cluster has one pixel that is sensitive to light intensity and three pixels with 0 degree, 45 degree and 90 degree gratings that are sensitive to incident light angles and polarization. The polarizer gratings were designed using the metal 1 layer and have a width of 100 nm which gives a pitch of 200 nm with a 50% duty cycle.

Figure 8a shows the response produced by unpolarized, 90° and 0° polarized light when incident on a 0° (horizontal) polarization pixel. As we had discussed earlier, light polarized orthogonal to the grating produces maximum response in the photodiode. In this case since the grating is 0°, 90° polarized light produces maximum response and 0° polarized light produces no response.

An alternative scenario is shown in figure 8b in which unpolarized, 90° and 0° polarized light are incident on a 90° (vertical) polarization pixel. As we already know by now, 0° polarized light produces maximum response and 90° polarized light produces no response.

The response in both the above cases were recorded by varying the incident light angle from $-45°$ to $+45°$ in steps of 5°. The response from polarization pixels show a clear cosine nature with the maximum value at 0° and decreasing thereafter for oblique incidence angles.

For unpolarized light, any of the polarization pixels in the cluster will be able to detect variations in the incidence angles. On the other hand, if light is polarized we require at least two orthogonally polarized pixel gratings for angle detection. In the case of polarized light a single pixel will be sensitive to both incidence angle variation and the state of polarized light. However, if we sum the response from two orthogonal polarization pixels, we remove its polarization dependence and its sensitivity will only be proportional to angle variations.

Figure 9 shows the plot based on FDTD simulation for unpolarized light incident on a 0° polarization pixel and 60° polarized light on 0° and 90° polarization pixels. When the light is polarized to 60°, it will have a stronger polarization component along the Y axis (90°) and a weaker component along the X axis (0°). Consequently, for a 0° polarization pixel the 60° polarized light produces a stronger response (because of a stronger Y component) and a weak response in the 90° polarization pixel (because of a weaker X component). As can be seen, the summed response is same as that produced by an unpolarized light source and can be used to determine the incident angle variations independent of the polarization state of the incident light.

The polarization pixel cluster includes an additional 45° grating for computing the Stoke's parameters [52] that can be used for determining the degree of polarization and the polarization angle. For the experiments presented here we only concern ourselves with the 0° and 90° polarization pixels, relegating an explanation for the usefulness of the 45° polarization pixel to another occasion.

D. Polarization-QPC Technique for Incident Light Angle Detection

It was noted earlier that by combining a high-sensitive, non-linear, periodic angular response with a low-sensitive, linear angular response we can achieve focal plane angle detection in an efficient manner using a smaller number of pixels as compared to the conventional techniques. Keeping in line with this trend, we propose another technique which combines the polarization pixel response along with the QPC

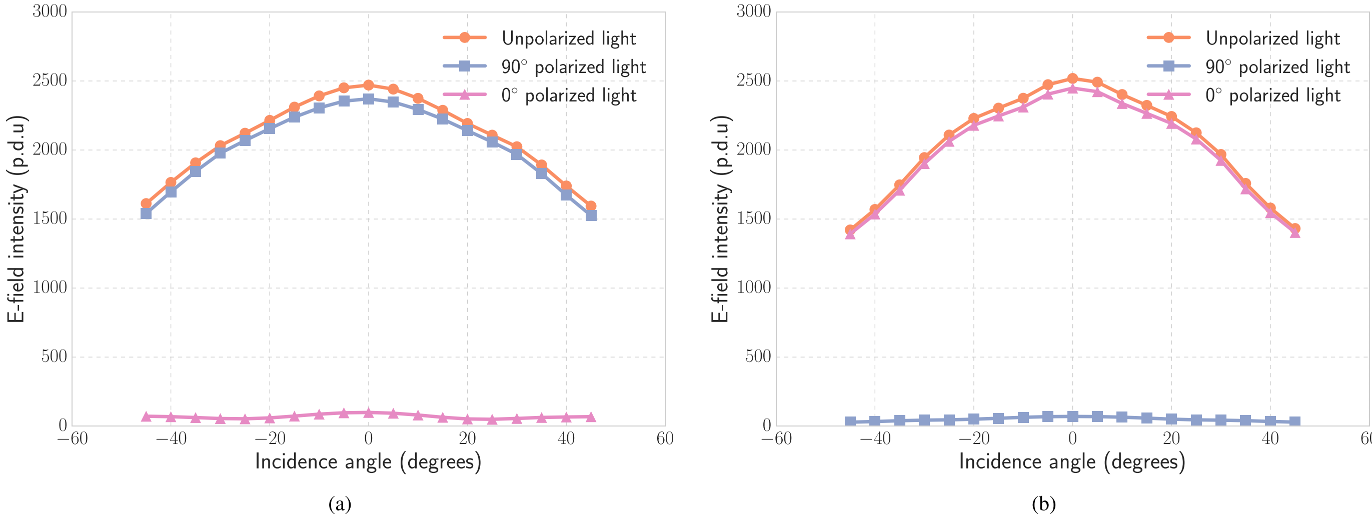

Fig. 8. Electric field intensity versus incidence angle variation for 0° (a) and 90° (b) polarization pixels under unpolarized light, 90° or vertically polarized light and 0° or horizontally polarized light.

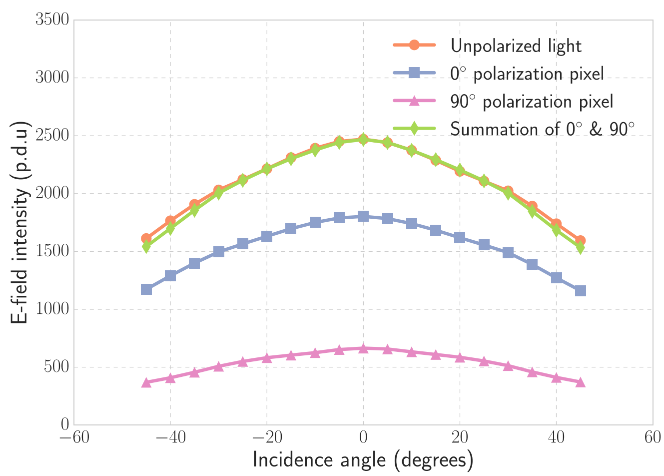

Fig. 9. Electric field intensity versus incidence angle variation of unpolarized light on 0° polarization pixel as comapred with 60° polarized light on 0° and 90° polarization pixels along with the summed response of 0° and 90° polarization pixels.

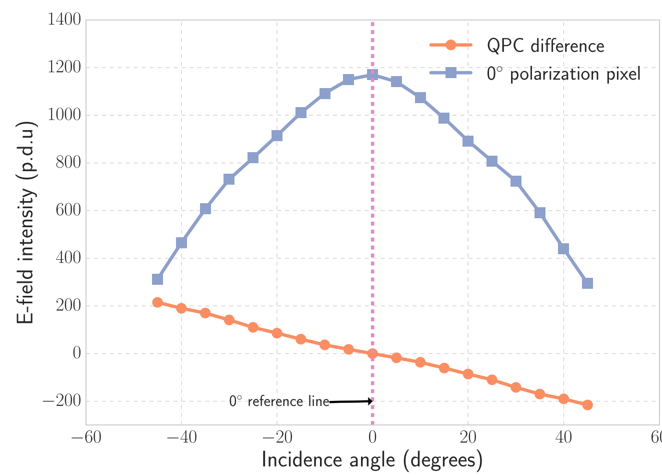

Fig. 10. Electric field intensity versus incidence angle variation of unpolarized light on 0° polarization pixel as compared to the QPC pixel response.

difference response to determine local incidence angle with high accuracy.

As was noted in the previous section, polarization pixels respond strongly to changes in incidence angles, but as seen from the figures (8a and 8b) their response is inherently symmetrical around 0 degrees. That is, with just the polarization pixel response it would be impossible to determine whether the incident angle is positive or negative. This is where the QPC difference response comes into play. The QPC response is linear as was previously noted, but their sensitivity to angle change is quite small. Hence by combining the highly angle sensitive, but symmetrical polarization response with QPC response of lower sensitivity, we can efficiently determine the local angle at the pixel level. This technique consumes only a smaller number of pixels thereby effectively increasing the spatial resolution of the sensor.

The technique is illustrated in figure 10. In the FDTD simulation, incident light angle was varied along the horizontal direction and QPC difference response and polarization response was recorded. Positive values of the QPC response indicates negative incident angles and negative values of the QPC response indicates positive incident angles. Once we know the coarse direction of light we can use the highly angle sensitive response of the polarization pixel to accurately determine the incident angle.

Since the polarization response is strongly sensitive to incidence angle variations, changes as small as 1 or 2 degrees can be effectively measured. This is in contrast with the QPC pixels where only angles that are sufficiently far apart such as 10 degrees or even 5 degrees can be measured. By combining the two techniques, we break the inherent symmetry present in the polarization response while at the same time achieving a higher angular resolution.

IV. Prototype Angle Sensitive Polarization Sensor

We designed a prototype sensor in 65 nm CMOS mixed-signal process to test our hypothesis. Figure 11 shows the micro-photograph of the sensor and gives a general idea about

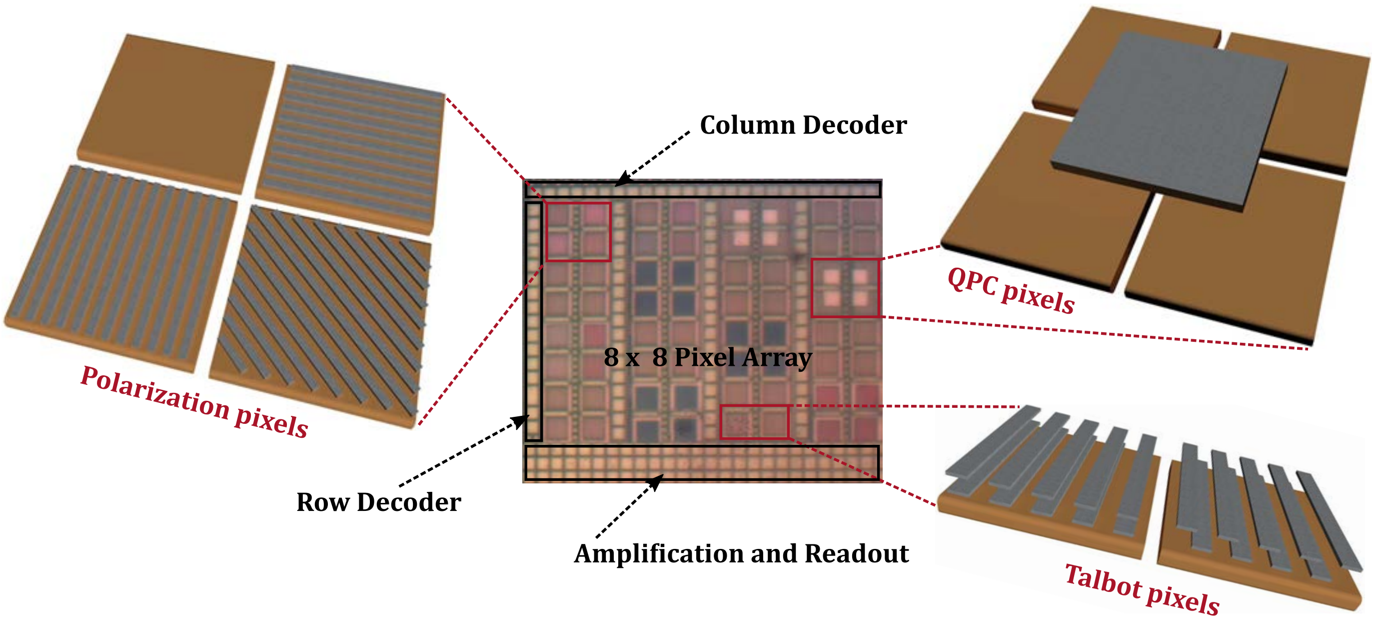

Fig. 11. Microphotograph showing sensor architecture along with the prominent pixel types in the sensor.

the sensor architecture. The sensor consists of 64 different pixel types, with the main ones described in this work shown by the blow-outs. The sensor consists of the polarization cluster and the QPC cluster described earlier along with eight Talbot pixels, four for each direction (X and Y) with grating offsets of 0, d/2, d/4 and 3d/4 which corresponds to α of 0, π, $\pi/2$ and $3\pi/2$ [9].

The pixels are made up of N-well/P-sub photodiode along with 3 transistors that make up a 3T APS pixel. The pixel occupies an area of 16.5 μm x 13 μm with the photodiode occupying an area of 10 μm x 10 μm giving rise to a fill factor of 46.6 %. The pixel merits a large photodiode since the on-pixel metal gratings block a huge portion of light falling on the pixel from reaching the photodiode. The on-pixel gratings also prevent the use of anti-reflection coatings on top of the pixels that are common in pixels fabricated using a custom image sensor process.

The polarization pixels have micro-polarizers that were implemented in metal 1 layer with a width of 100 nm and a pitch of 200 nm. QPC pixels have a metal block that was implemented in metal layer 5. The metal block covers the photodiode 6.5 μm along each of the X and Y directions. The primary grating of the Talbot pixel was implemented in metal layer 5 with a pitch of 0.76 μm which caused the self-images to occur at the depth of metal 1 layer. Metal 1 layer acts as the secondary grating and has the same pitch as the primary.

The pixel voltages are amplified by a factor of 2 by the global switched capacitor amplifier before being readout through a global buffer for further downstream processing. Important sensor parameters are listed in Table I.

TABLE I
IMPORTANT SENSOR PARAMETERS

Parameter	Value
Technology	65 nm, CMOS mixed-signal process
Pixel size	16.5 μm x 13 μm
Fill factor	46.6 %
Pixel structure	3T APS
Pixel power consumption	12.13 μW
Dark current	26.06 nA/cm^2
Temporal noise	1.48 mV
Dynamic range	61.77 dB
Full well capacity	505 Ke$^-$
Conversion gain	3.6 μV/e$^-$
Photodiode Sensitivity	0.325 V/lux-sec
Angular Sensitivity of QPC pixels	5.63 mV/deg
Angular Sensitivity of Talbot pixels	8.70 mV/deg
Angular Sensitivity of Polarization pixels	12.28 mV/deg
Supply voltage	3.3 V analog; 1.2 V digital

V. Test Setup and Testing Methodology

We tested the sensor for its response on incidence angle variations for multiple configurations of polarized and unpolarized light. Figure 12 shows the test setup in which the prototype sensor, mounted on a PCB board is attached to a single-axis rate table. By controlling the rate at with the table rotates and the time taken we can orient the sensor to have an angle with the incoming light rays from the sun simulator. The sun simulator placed at a distance of 5 meters from the PCB setup produces collimated rays of light over a broad range of wavelengths from 300 nm to 1000 nm.

The raw data from the sensor is converted to its digital equivalent by an external ADC and captured by an Opal Kelly board. The data is then sent to a computer for further processing.

For experiments on incident angle variations, the rate-table was rotated in steps of 5 degrees exposing the sensor to varying angles of collimated rays from the sun simulator.

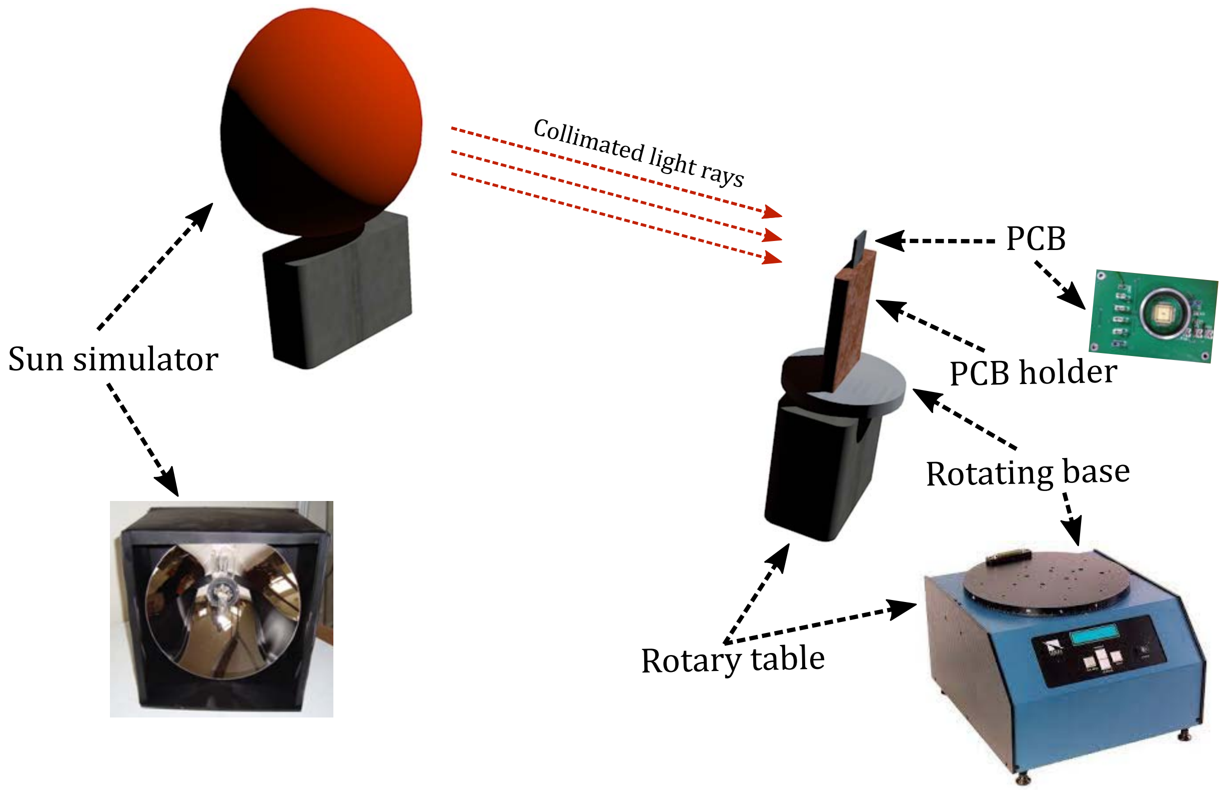

Fig. 12. Testing arrangement showing a sun simulator illuminating the prototype sensor placed on a single-axis rate table.

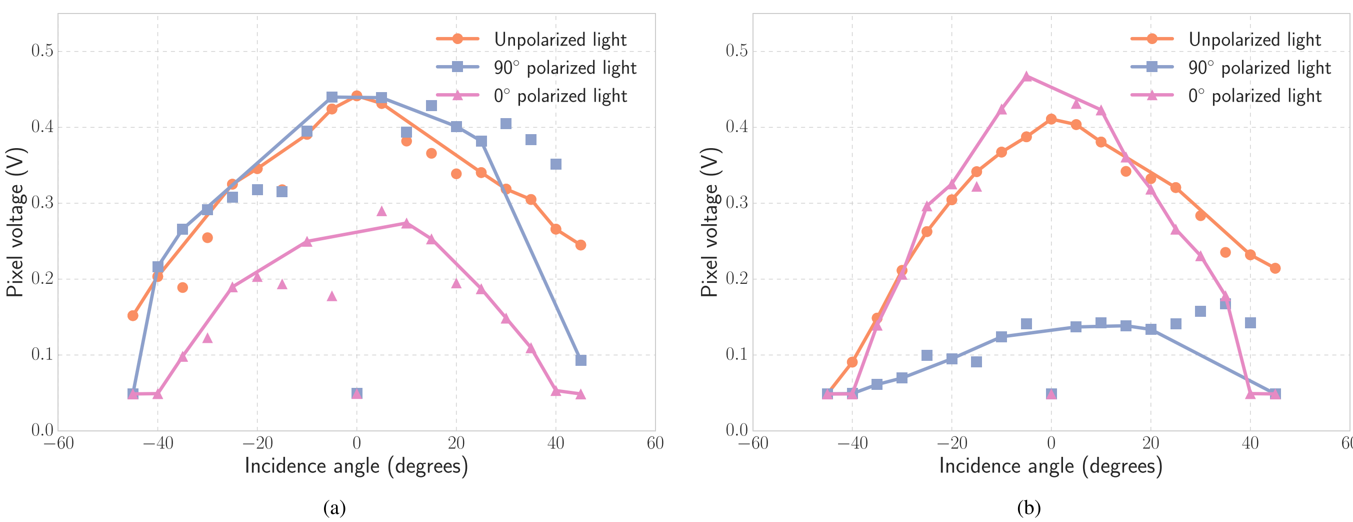

Fig. 13. Pixel voltage versus incidence angle variation for 0° (a) and 90° (b) polarization pixels under unpolarized light, 90° or vertically polarized light and 0° or horizontally polarized light.

VI. Experimental Results

We have extensively characterized the sensor for incident angle variations under various polarization conditions. Some of the results are presented in the following sections.

A. Characterization of Polarization Pixels

For characterizing the polarization pixels we varied the incident light angle from $-45°$ to $+45°$ in steps of 5° and measured the recorded response.

Figure 13a shows the response produced by a 0° polarization pixel for unpolarized, 90° polarized and 0° polarized light. As we had observed with the FDTD simulations, the response of the pixel for light polarized orthogonal (90° polarized light) to the grating is maximum. While light polarized parallel (0° polarized light) to the grating is minimum.

Similarly figure 13b shows the response produced by a 90° polarization pixel for unpolarized, 90° polarized and 0° polarized light. In this case again response for light

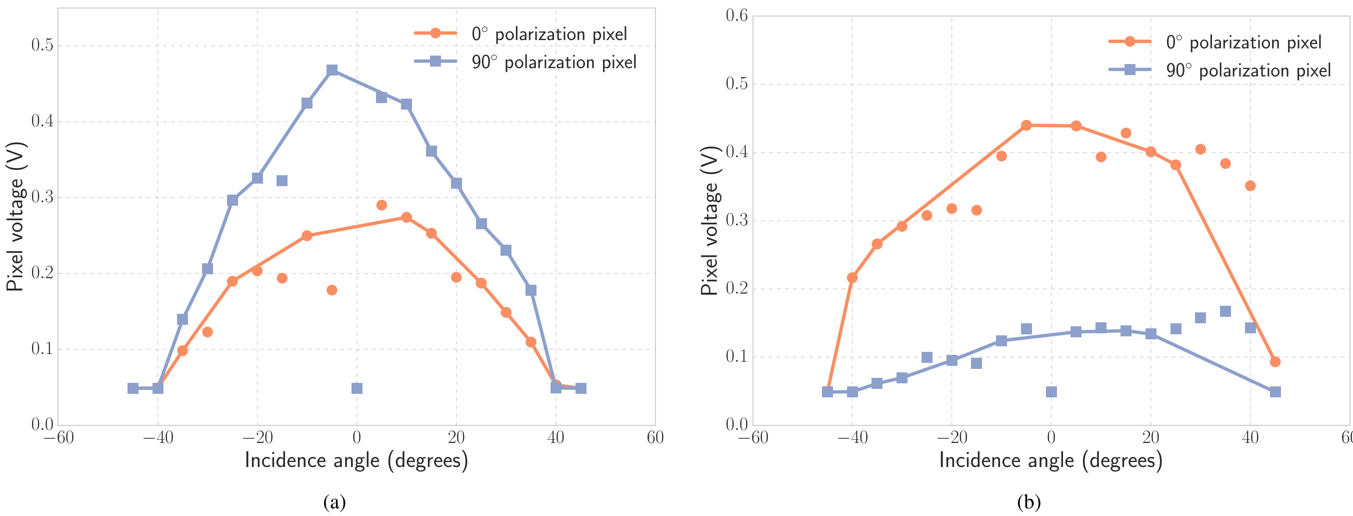

Fig. 14. Pixel voltage versus incidence angle variation for 0° and 90° polarization pixels under 0° or horizontally polarized light (a) and 90° or vertically polarized light (b).

polarized orthogonal (0° polarized light) to the grating is maximum. While light polarized parallel (90° polarized light) to the grating is minimum.

Figures 14 and 15 reinterpret the above results in a slightly different manner for better clarity. Figure 14a shows the response produced by 0° polarized light when incident on 0° and 90° polarization pixels. For a 0° polarized light, 0° polarization pixel produces minimum response whereas 90° polarization pixel produces maximum response.

In a similar manner figure 14b shows the response produced by 90° polarized light when incident on 0° and 90° polarization pixels. For 90° polarized light, 0° polarization pixel produces maximum response whereas 90° polarization pixel produces minimum response.

Figure 15 shows the response produced by unpolarized light when incident on 0° and 90° polarization pixels, which is in agreement with the theory that the response produced by polarization gratings of random orientations to unpolarized light is equal.

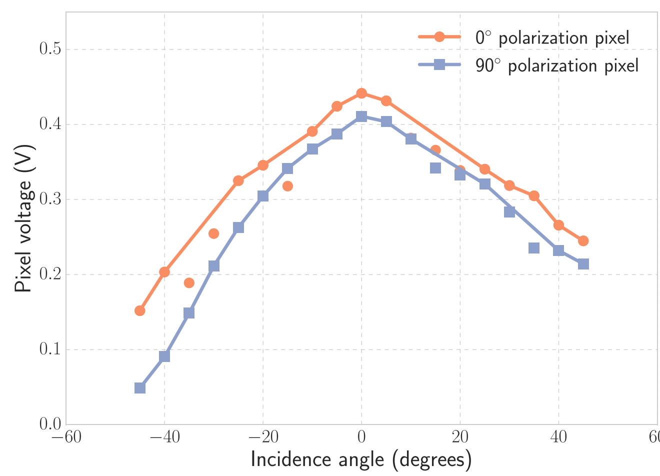

Fig. 15. Pixel voltage versus incidence angle variation for 0° and 90° polarization pixels under unpolarized light.

B. Comparing Polarization, Talbot and QPC Pixel responses

Figure 16 contrasts the response produced by Polarization, Talbot and QPC pixels. The responses were recored by varying incident light angle horizontally (along X axis) from −45° to +45° in steps of 5°. We have used a 90° polarization pixel with 0° polarized light for comparison.

As expected the difference response from the QPC pixels (along X direction) is linear. The response from polarization pixel has a cosine nature and that from the Talbot pixel is periodic, with its periodicity dependent on the grating parameters.

As seen from the plot, the angle sensitivity of the polarization and Talbot pixels are higher than the QPC pixels. The sensitivity of an angle sensitive pixel can be defined as the response produced by the pixel for one degree change in incident light angle. It can be expressed in mV/deg. Table I gives the angle sensitivities for each of the pixel types.

The periodic nature of the Talbot response requires multiple angle-uwrappings with aid from the QPC response in order to decode the incident angle. Polarization response on the other hand is a simple cosine curve with a peak at 0° and requires just one angle-unwrappping to uniquely decode the incident light angle.

C. Angle Detection Using Polarization and QPC Pixels

The principle of angle detection using polarization and QPC pixel was introduced in section III. We illustrate the same here with experimental results. Figure 17 shows the polarization pixel response and the QPC pixel response from the previous subsection. As seen from the figure positive voltages of the QPC response indicates that the incident angle is negative and negative voltages of the QPC response indicates that the incident angle is positive.

Once we know the sign of the incident angle (positive or negative) we can use the corresponding half of the polarization

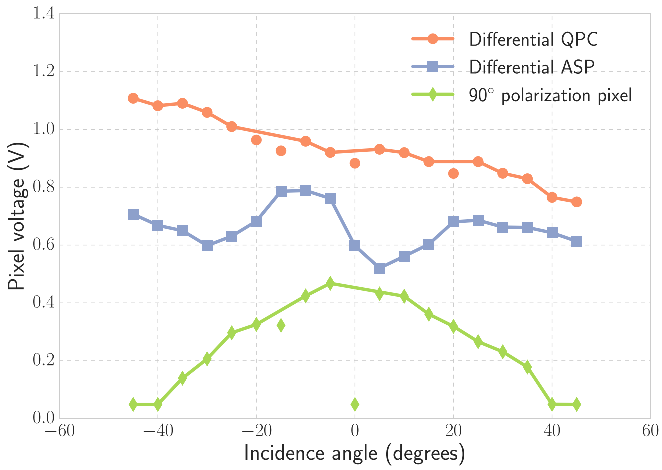

Fig. 16. Pixel voltage versus incidence angle variation of differential quadrature pixel cluster (QPC), differential Talbot effect based angle sensitve pixel (ASP) and 90° polarization pixel.

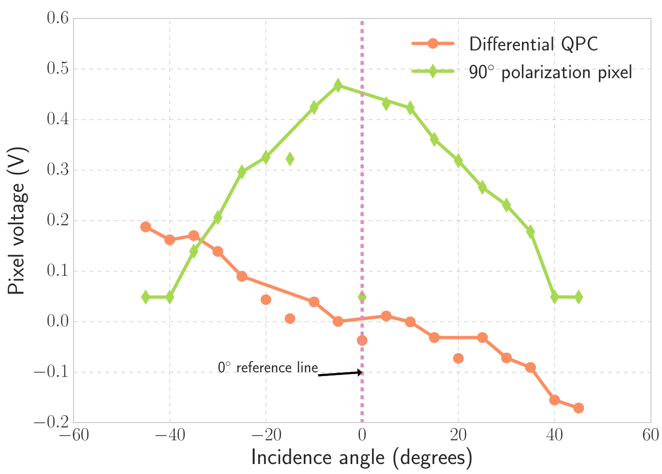

Fig. 17. Pixel voltage versus incidence angle variation of differential quadrature pixel cluster (QPC) and 90° polarization pixel illustrating the angle detection technique.

response to get an accurate value of the incident light angle.

VII. Discussion

Several factors contribute to the nonidealities in the results obtained from the prototype sensor. Some factors are a result of the pixel design and others are a result of the limitations in the experimental setup. We discuss some of these factors here.

A. Design Limitations

Design limitations are either due to the restrictions in designing an image sensor pixel or the inherent limitations in the CMOS fabrication process.

1) Optical Pixel Crosstalk: Optical Pixel crosstalk [53] results when light meant for one pixel falls on its adjacent neighbor thereby producing unwanted response. For large positive and negative angles crosstalk could become a serious issue which increases the angle insensitive baseline pixel response. This in fact reduces the per-degree angle sensitivity of a particular pixel. This could be one of the issues that contribute to the less than ideal characteristic of the pixel response at large positive or negative angles.

2) Pixel Vignetting: Pixel vignetting [54] is another factor that contributes to the angle dependent nature of a pixel and is a result of the interconnect metal layers in the vicinity of the photodiode. Typically, pixel vignetting is influenced more by the light-shield around the photodiode that is used to enforce uniformity along all the photodiode directions to incident light rays.

For normal incidence, there is no shadow on the photodiode because of the light shield and the photodiode produces maximum response. On the other hand, for oblique angles the response reduces as a function of the incident light angle.

The above limitations are a result of the pixel architecture and are difficult to eliminate under normal circumstances. For example, in order to reduce pixel crosstalk, the pixels have to be placed very far apart, which in fact is not practical as it increases the sensor area without increasing the sensor pixel resolution. Similarly pixel vignetting can be reduced by eliminating any metal layers in the vicinity of the photodiode. This again is not practical as it would require a large pixel size and is not feasible because of the above mentioned reason.

B. Experimental Limitations

These limitations arise because of the inefficiencies in the test setup and testing methodology.

1) Lambert's Cosine Law: Lambert's cosine law states that the light incident on a surface with a fixed area at an oblique angle of incidence is equal to the cosine of its value at normal incidence. This is given as $I(\theta) = I(0)\mathrm{Cos}(\theta)$. The consequence of this law is that, when the light source is wider than the pixel and the incident angle is θ, which is not 0°, the optical power on the surface of the photodiode decreases as the angle increases. This introduces an angle dependent behavior for a conventional intensity pixel. The effect of just the cosine law on the angle sensitivity of a pixel is very weak and is a non-issue when a lens is introduced to focus the light beam, unlike in the present scenario.

2) Sensor-Light Source Alignment: Misalignment between the sensor and the sun-simulator (light source) will introduce a slight angle dependence to the recorded responses.

3) Control of Angle Variation: The angle made by the sensor with the light source was varied by letting the rotary table rotate at a fixed rate for a particular amount of time. Even though the rotation was controlled by a PC, latencies in the instruction execution pipeline adversely impacted the angle variation of the rotary table.

4) Ray Divergence: The collimated light ray from the sun simulator diverges from its normal angle at distances away from the sun simulator. The amount of divergence depends on the actual distance between the sensor and the sun simulator and could have been a small contributing factor to inaccurate angle measurements.

5) Temperature Effects: At small distances from the sun simulator, the ambient temperature increases to a non-negligible amount. Prolonged operation of the sun simulator results in a sharp increase of the sensor dark current.

6) Unwanted Polarizaton of Light: The sun simulator has a glass-covering around its outer edge and it contributed to a slight polarization of the incident light. Hence light from the sun simulator was partially polarized with a small horizontal polarization component instead of being completely unpolarized.

VIII. Conclusion

In this paper we have presented a polarization based technique for detecting the incoming light ray direction and its angle with respect to the image sensor normal. This technique combines the highly sensitive, non linear response of the polarization pixels with the not-so-sensitive, linear response of the quadrature pixel cluster (QPC) pixels to accurately determine the incident light angles. Determining the light angle gives one the ability to know the position of the object with respect to the focal plane of the lens, which helps us in post capture refocus and synthetic aperture photography. The presented technique uses only 7 pixels, as opposed to the 13 used by the earlier track-and-tune technique to determine the light angle. This technique also simplifies the post processing needed to detect the angle as only one angle unwrapping is required as opposed to the Talbot pixels that require 3-4 angle unwrapping's.

Acknowledgement

The authors would like to acknowledge Tao Jin, Liang Guozhen, and Qi Jie Wang from Division of Microelectronics, School of Electrical and Electronic Engineering, Nanyang Technological University for helpful discussions.

References

[1] G. Lippmann, "Epreuves reversible donnant la sensation du relief," *J. Phys.*, vol. 7, no. 4, pp. 821–825, Nov. 1908.

[2] H. E. Ives, "Parallax panoramagrams made with a large diameter lens," *J. Opt. Soc. Amer.*, vol. 20, no. 6, pp. 332–342, Jun. 1930.

[3] K. Fife, A. El Gamal, and H.-S. P. Wong, "A 3D multi-aperture image sensor architecture," in *Proc. IEEE Custom Integr. Circuits Conf. (CICC)*, Sep. 2006, pp. 281–284.

[4] K. Fife, A. El Gamal, and H.-S. P. Wong, "A 3MPixel multi-aperture image sensor with 0.7 μm pixels in 0.11 μm CMOS," in *Proc. IEEE Int. Solid-State Circuits Conf. Dig. Tech. Papers (ISSCC)*, Feb. 2008, pp. 48–594.

[5] R. Ng, "Digital light field photography," Ph.D. dissertation, Dept. Comput. Sci., Stanford Univ., Stanford, CA, USA, 2006.

[6] T. Georgeiv, K. C. Zheng, B. Curless, D. Salesin, S. Nayar, and C. Intwala, "Spatio-angular resolution tradeoff in integral photography," in *Proc. 17th Eurograph. Conf. Rendering Techn. (EGSR)*, Aire-la-Ville, Switzerland, 2006, pp. 263–272.

[7] E. H. Adelson and J. Y. A. Wang, "Single lens stereo with a plenoptic camera," *IEEE Trans. Pattern Anal. Mach. Intell.*, vol. 14, no. 2, pp. 99–106, Feb. 1992.

[8] K. Fife, A. El Gamal, and H.-S. P. Wong, "A multi-aperture image sensor with 0.7 μm pixels in 0.11 μm CMOS technology," *IEEE J. Solid-State Circuits*, vol. 43, no. 12, pp. 2990–3005, Dec. 2008.

[9] A. Wang and A. Molnar, "A light-field image sensor in 180 nm CMOS," *IEEE J. Solid-State Circuits*, vol. 47, no. 1, pp. 257–271, Jan. 2012.

[10] A. Wang, P. Gill, and A. Molnar, "Light field image sensors based on the Talbot effect," *Appl. Opt.*, vol. 48, no. 31, pp. 5897–5905, Nov. 2009. [Online]. Available: http://ao.osa.org/abstract.cfm?URI=ao-48-31-5897

[11] A. Wang, P. R. Gill, and A. Molnar, "Angle sensitive pixels in CMOS for lensless 3D imaging," in *Proc. IEEE Custom Integr. Circuits Conf. (CICC)*, Sep. 2009, pp. 371–374.

[12] A. Wang, P. R. Gill, and A. Molnar, "Fluorescent imaging and localization with angle sensitive pixel arrays in standard CMOS," in *Proc. IEEE Sensors*, Nov. 2010, pp. 1706–1709.

[13] A. Wang, S. Sivaramakrishnan, and A. Molnar, "A 180 nm CMOS image sensor with on-chip optoelectronic image compression," in *Proc. IEEE Custom Integr. Circuits Conf. (CICC)*, Sep. 2012, pp. 1–4.

[14] A. Wang, P. R. Gill, and A. Molnar, "An angle-sensitive CMOS imager for single-sensor 3D photography," in *Proc. IEEE Int. Solid-State Circuits Conf. Dig. Tech. Papers (ISSCC)*, Feb. 2011, pp. 412–414.

[15] H. F. Talbot, "LXXVI. Facts relating to optical science. No. IV," *Philos. Mag.*, vol. 9, no. 56, pp. 401–407, 1836.

[16] V. Varghese *et al.*, "Track-and-tune light field image sensor," *IEEE Sensors J.*, vol. 14, no. 12, pp. 4372–4384, Dec. 2014.

[17] C. Koch, J. Oehm, and A. Gornik, "High precision optical angle measuring method applicable in standard CMOS technology," in *Proc. ESSCIRC*, Sep. 2009, pp. 244–247.

[18] C. Koch, J. Oehm, J. Emde, and W. Budde, "Light source position measurement technique applicable in SOI technology," *IEEE J. Solid-State Circuits*, vol. 43, no. 7, pp. 1588–1593, Jul. 2008.

[19] V. Varghese, X. Qian, S. Chen, and S. ZeXiang, "Linear angle sensitive pixels for 4D light field capture," in *Proc. Int. SoC Design Conf. (ISOCC)*, Nov. 2013, pp. 072–075.

[20] V. Varghese and S. Chen, "Incident light angle detection technique using polarization pixels," in *Proc. IEEE SENSORS*, Nov. 2014, pp. 2167–2170.

[21] T. Waterman, "Polarization sensitivity," in *Handbook of Sensory Physiology, Part 6b: Vision of Invertebrates*, vol. 7, H. J. Altrum ed. Berlin, Germany: Springer-Verlag, 1981, pp. 283–463.

[22] R. M. Glantz, "Polarization analysis in the crayfish visual system," *J. Experim. Biol.*, vol. 204, no. 14, pp. 2383–2390, 2001.

[23] J. C. Tuthill and S. Johnsen, "Polarization sensitivity in the red swamp crayfish Procambarus clarkii enhances the detection of moving transparent object," *J. Experim. Biol.*, vol. 209, no. 9, pp. 1612–1616, 2006.

[24] M. Dacke, T. A. Doan, and D. C. O'Carroll, "Polarized light detection in spiders," *J. Experim. Biol.*, vol. 204, no. 14, pp. 2481–2490, 2001.

[25] M. Müller and R. Wehner, "The hidden spiral: Systematic search and path integration in desert ants, *Cataglyphis fortis*," *J. Comparative Physiol. A*, vol. 175, no. 5, pp. 525–530, 1994.

[26] U. Homberg, S. Heinze, K. Pfeiffer, M. Kinoshita, and B. el Jundi, "Central neural coding of sky polarization in insects," *Philos. Trans. Roy. Soc. London B, Biol. Sci.*, vol. 366, no. 1565, pp. 680–687, 2011.

[27] K. Adler and J. B. Phillips, "Orientation in a desert lizard (Uma notata): Time-compensated compass movement and polarotaxis," *J. Comparative Physiol. A*, vol. 156, no. 4, pp. 547–552, 1985.

[28] C. W. Hawryshyn, "Ultraviolet-polarization vision: Its role in salmon navigation," *Proc. SPIE*, vol. 3120, pp. 2–10, Dec. 1997.

[29] R. Wehner, B. Michel, and P. Antonsen, "Visual navigation in insects: Coupling of egocentric and geocentric information," *J. Experim. Biol.*, vol. 199, no. 1, pp. 129–140, 1996.

[30] L. B. Wolff, "Polarization-based material classification from specular reflection," *IEEE Trans. Pattern Anal. Mach. Intell.*, vol. 12, no. 11, pp. 1059–1071, Nov. 1990.

[31] M. Sarkar, D. San Segundo Bello, C. Van Hoof, and A. Theuwissen, "Integrated polarization analyzing CMOS image sensor for material classification," *IEEE Sensors J.*, vol. 11, no. 8, pp. 1692–1703, Aug. 2011.

[32] M. Sarkar, D. San Segundo Bello, C. Van Hoof, and A. Theuwissen, "Integrated polarization-analyzing CMOS image sensor for detecting incoming light ray direction," in *Proc. IEEE Sensors Appl. Symp. (SAS)*, Feb. 2010, pp. 194–199.

[33] S. Makita, Y. Yasuno, T. Endo, M. Itoh, and T. Yatagai, "Polarization contrast imaging of biological tissues by polarization-sensitive Fourier-domain optical coherence tomography," *Appl. Opt.*, vol. 45, no. 6, pp. 1142–1147, Feb. 2006.

[34] S.-S. Lin, K. M. Yemelyanov, E. N. Pugh, and N. Engheta, "Polarization-based and specular-reflection-based noncontact latent fingerprint imaging and lifting," *J. Opt. Soc. Amer. A*, vol. 23, no. 9, pp. 2137–2153, Sep. 2006.

[35] Y. Y. Schechner, S. G. Narasimhan, and S. K. Nayar, "Polarization-based vision through haze," *Appl. Opt.*, vol. 42, no. 3, pp. 511–525, Jan. 2003.

[36] O. Morel, F. Meriaudeau, C. Stolz, and P. Gorria, "Polarization imaging applied to 3D reconstruction of specular metallic surfaces," *Proc. SPIE*, vol. 5679, pp. 178–186, Mar. 2005.

[37] A. G. Andreou and Z. K. Kalayjian, "Polarization imaging: Principles and integrated polarimeters," *IEEE Sensors J.*, vol. 2, no. 6, pp. 566–576, Dec. 2002.

[38] M. Kulkarni and V. Gruev, "A division-of-focal-plane spectral-polarization imaging sensor," *Proc. SPIE*, vol. 8364, pp. 83640K-1–83640K-11, Jun. 2012. [Online]. Available: http://dx.doi.org/10.1117/12.919143

[39] V. L. Gamiz, “Performance of a four-channel polarimeter with low-light-level detection,” *Proc. SPIE*, vol. 3121, pp. 35–46, Oct. 1997.

[40] E. Hecht, *Optics*, 4th ed. Reading, MA, USA: Addison-Wesley, 2002.

[41] M. Zhang, X. Wu, N. Cui, N. Engheta, and J. Van der Spiegel, “Bioinspired focal-plane polarization image sensor design: From application to implementation,” *Proc. IEEE*, vol. 102, no. 10, pp. 1435–1449, Oct. 2014.

[42] M. Zhang, X. Wu, N. Engheta, and J. Van der Spiegel, “A monolithic CMOS image sensor with wire-grid polarizer filter mosaic in the focal plane,” *IEEE Trans. Electron Devices*, vol. 61, no. 3, pp. 855–862, Mar. 2014.

[43] A. Gershun, “The light field,” *J. Math. Phys.*, vol. 18, nos. 1–4, pp. 51–151, 1939.

[44] E. H. Adelson and J. R. Bergen, “The plenoptic function and the elements of early vision,” in *Computational Models of Visual Processing*. Cambridge, MA, USA: MIT Press, 1991, pp. 3–20.

[45] M. Levoy and P. Hanrahan, “Light field rendering,” in *Proc. 23rd Annu. Conf. Comput. Graph. Interact. Techn. SIGGRAPH*, New York, NY, USA, 1996, pp. 31–42. [Online]. Available: http://doi.acm.org/10.1145/237170.237199

[46] S. J. Gortler, R. Grzeszczuk, R. Szeliski, and M. F. Cohen, “The lumigraph,” in *Proc. 23rd Annu. Conf. Comput. Graph. Interact. Techn. SIGGRAPH*, New York, NY, USA, 1996, pp. 43–54. [Online]. Available: http://doi.acm.org/10.1145/237170.237200

[47] A. Isaksen, L. McMillan, and S. J. Gortler, “Dynamically reparameterized light fields,” in *Proc. 27th Annu. Conf. Comput. Graph. Interact. Techn. SIGGRAPH*, New York, NY, USA, 2000, pp. 297–306.

[48] A. Veeraraghavan, R. Raskar, A. Agrawal, A. Mohan, and J. Tumblin, “Dappled photography: Mask enhanced cameras for heterodyned light fields and coded aperture refocusing,” *ACM Trans. Graph.*, vol. 26, no. 3, 2007, Art. no. 69.

[49] K. Marwah, G. Wetzstein, Y. Bando, and R. Raskar, “Compressive light field photography using overcomplete dictionaries and optimized projections,” *ACM Trans. Graph.*, vol. 32, no. 4, 2013, Art. no. 46.

[50] A. Molnar and A. Wang, “Light field image sensor, method and applications,” U.S. Patent 20 110 174 998 A1, Jul. 21, 2011.

[51] M. Testorf, J. Jahns, N. A. Khilo, and A. M. Goncharenko, “Talbot effect for oblique angle of light propagation,” *Opt. Commun.*, vol. 129, nos. 3–4, pp. 167–172, 1996. [Online]. Available: http://www.sciencedirect.com/science/article/pii/0030401896001319

[52] M. Sarkar, D. San Segundo Bello, C. Van Hoof, and A. J. P. Theuwissen, “Integrated polarization-analyzing CMOS image sensor for detecting the incoming light ray direction,” *IEEE Trans. Instrum. Meas.*, vol. 60, no. 8, pp. 2759–2767, Aug. 2011.

[53] L. Blockstein and O. Yadid-Pecht, “Crosstalk quantification, analysis, and trends in CMOS image sensors,” *Appl. Opt.*, vol. 49, no. 24, pp. 4483–4488, Aug. 2010.

[54] P. B. Catrysse, X. Liu, and A. El Gamal, “QE reduction due to pixel vignetting in CMOS image sensors,” *Proc. SPIE*, vol. 3965, pp. 420–430, May 2000.